FastReg: Fast Non-Rigid Registration via Accelerated Optimisation on the Manifold of Diffeomorphisms

Daniel Grzech[1], Loïc Le Folgoc[1], Mattias P. Heinrich[2], Bishesh Khanal[3], Jakub Moll[4], Julia A. Schnabel[2], Ben Glocker[1], and Bernhard Kainz[1]

[1] Department of Computing, Imperial College London, London, UK
{d.grzech17,l.le-folgoc,b.glocker,b.kainz}@imperial.ac.uk
[2] Institute of Medical Informatics, University of Luebeck, Luebeck, Germany
heinrich@imi.uni-luebeck.de
[3] School of Biomedical Engineering and Imaging Sciences, King's College London, London, UK {bishesh.khanal,julia.schnabel}@kcl.ac.uk
[4] International Medical School, University of Milan, Milan, Italy
jakub.moll@studenti.unimi.it

Abstract. We present a new approach to diffeomorphic non-rigid registration of medical images. The method is based on optical flow and warps images via gradient flow with the standard L^2 inner product. To compute the transformation, we rely on accelerated optimisation on the manifold of diffeomorphisms. We achieve regularity properties of Sobolev gradient flows, which are expensive to compute, owing to a novel method of averaging the gradients in time rather than space. We successfully register brain MRI and challenging abdominal CT scans at speeds orders of magnitude faster than previous approaches. We make our code available in a public repository: https://github.com/dgrzech/fastreg.

1 Introduction

Medical imaging research has led to excellent solutions to problems such as volumetric brain registration [12,21], thoracic CT registration [34], and cardiac MRI registration [24]. However, making a registration algorithm fast and applicable to a wide range of imaging modalities, organs, and settings, e.g. longitudinal vs cross-sectional data, is still an open problem. For instance, popular registration methods tend to fail in case of abdominal CT scans [39]. The difficulty of abdominal CT is the result of inter-subject variability, e.g. due to age, gender, and weight, and variation in inter-organ relationships, e.g. due to pose, respiratory cycles, and illness. Moreover, open-source registration tools leave a lot to be desired in terms of processing speed.

In parallel to new developments in image registration on the medical front, in recent years optical flow has been a hot topic in computer vision. Variational methods and deep learning models for optical flow are becoming more accurate, more robust, and faster [5,14], and are finding use in new applications, such as deformable 3D scene reconstruction [29,28].

In this work we build on the latest research in optical flow to address the problems of medical image registration robustness, accuracy, and speed by employing a novel method of accelerated optimisation on infinite-dimensional manifolds, in particular the manifold of diffeomorphisms. We propose using a new optimiser to solve the optical flow problem in a variational setting, allowing us to minimise the energy functional at a reduced computational cost. Thus we achieve processing speeds which are orders of magnitude faster than in other tools for medical image registration, without compromising on the accuracy. We show that the method is successful on the challenging tasks of registration of abdominal CT scans and of brain MRI scans, paving the way to new clinical applications of medical image registration. The main highlights of our contribution are:

1. We introduce FastReg, a system for medical image registration that leverages recent advances in non-convex optimisation.
2. We build on the latest research in optimisation, which generalises the concept of Nesterov accelerated momentum to infinite-dimensional manifolds, to design and implement a new tool for non-rigid diffeomorphic image registration.
3. Our approach is significantly faster than previous non-rigid registration methods, while outperforming most of them in terms of the Dice segmentation overlap on the registration of challenging abdominal CT scans with multi-organ segmentations, and of brain MRI with tissue segmentations.
4. The presented framework is highly suitable for parallelisation and we provide a publicly available implementation, which makes use of GPU acceleration.

2 Related work

Non-rigid medical image registration. Non-rigid registration is a key element in many clinical imaging applications. Prominent examples include population-based studies, both cross-sectional and longitudinal, on brain image data from magnetic resonance imaging (MRI) and morphometric applications that require images to be mapped into a canonical space. Registration to canonical spaces allows to characterise morphological changes and has helped gain new insight in diseases such as Alzheimer's disease [18,19] and cancer [4].

Variants of free-form deformation (FFD) algorithms [25] have long been popular for non-rigid registration methods, with improvements mainly due to more efficient implementations, e.g. using GPUs [22]. However, the difficulty of computing smooth deformation fields between semantically similar structures, e.g. in the presence of local motion discontinuities due to sliding motion between organs, has been a major obstacle in clinical applications [26].

In drop [8] this problem was mitigated by reformulating the continuous domain of FFD algorithms in order to enable the use of fast discrete optimisation. In DEEDS [11], the ideas used in drop have been further enhanced with elements that allow for more complex motion modelling.

Conversely, the demons algorithm and its variants [33,35,17] propose a parameterisation of deformations derived from optical flow. These approaches are promising for enabling accurate solutions, but sometimes suffer from limited

robustness due to discretisation issues of the continuous demons domain [36]. Computational bottlenecks also remain challenging, especially for applications with real-time constraints.

Accelerated optimisation. Accelerated optimisation methods are widely used in machine learning. They include e.g. Nesterov accelerated gradient descent [23], Adadelta [40], and Adagrad [6]. For convex problems, they are known to produce optimal convergence rates among first-order optimisation schemes. Recently, the class of functions where linear convergence is possible only with first-order information has been expanded to include non-strongly convex functions [20]. Meanwhile, in the non-convex case, accelerated gradient descent is used to provide robustness to local minima. However, these acceleration methods are only valid for optimisation problems in finite dimensions, which makes them unsuitable for variational problems.

In optical flow and segmentation applications, the non-convex nature of the problem is often addressed via inverse differential operators. Sobolev gradients [32] which make gradient descent robust to shallow local minima have been successfully used for a wide range of tasks in computer vision, including image interpolation [15] and image registration [2,3]. However, the computation of inverse differential operators is expensive in practice, involves a number of approximations, and proved to be a bottleneck in uses where speed is a critical factor. In [30], authors of the work on Sobolev active contours [31] outlined a new method to accelerate optimisation on infinite dimensional manifolds, e.g. that of diffeomorphisms, which produces a similar effect to Sobolev gradients without the spatial averaging of gradients. The new method is itself an extension of a general class of accelerated optimisation methods for finite-dimensional variational problems proposed in [37]. These novel accelerated schemes for variational optimisation are the core of our system.

3 Method

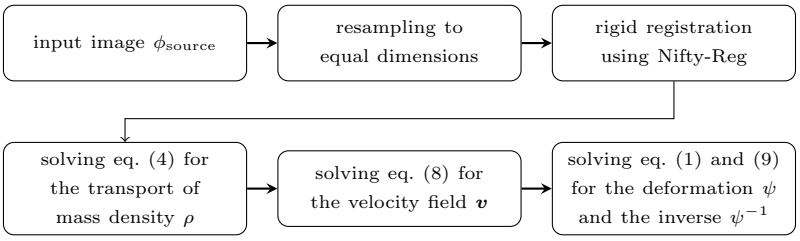

Fig. 1: System overview. We calculate the deformation by solving a number of partial differential equations through integration. Updates to the mass density ρ, velocity field $\boldsymbol{v}$, and deformation fields ψ and ψ^{-1} are all local, which allows to process each voxel independently and in parallel.

The volumes to be registered consist of voxel grids indexed by triples $\boldsymbol{r} = (x, y, z) \in \mathbb{N}^3$. We rescale the image intensities to the interval $[0, 1]$.

For each ϕ_{source}, we calculate the diffeomorphism $\psi : \mathbb{N}^3 \to \mathbb{R}^3$ that aligns the source image to the reference image, i.e. $\phi_{\text{source}} \circ \psi = \phi_{\text{target}}$, and the inverse diffeomorphism $\psi^{-1} : \mathbb{N}^3 \to \mathbb{R}^3$ that aligns the reference image to the source image, i.e. $\phi_{\text{source}} = \phi_{\text{reference}} \circ \psi^{-1}$.

4 Optimisation

In image registration and optical flow, standard gradient descent is prone to get stuck in numerical local minima and so requires significant data pre-processing. Sobolev gradients are a popular way around this but involve expensive computation of inverse differential operators. Here we describe how accelerated optimisation on the manifold of diffeomorphisms allows to derive local evolution equations, which overcome issues associated with vanilla gradient descent. We obtain robustness properties of Sobolev gradients but without use of spatial convolution, which is a major computational bottleneck in methods which use them. This leads to a significant speed-up over previous registration methods and enables fast registration at higher resolutions.

The main idea of the accelerated optimisation scheme can be summarised as follows. To compute the transformation, we use an energy consisting of a potential term and a kinetic term. The potential term is the motor of the registration and allows to align the images. The kinetic term endows the scheme with dynamics and keeps the solver from getting stuck in shallow local minima. It models the evolution of an infinite number of particles represented by a mass density, which is evolved with the transformation.

In what follows, we make use of the result that any diffeomorphism can be generated by integrating a smooth time-varying vector field over time [7]. Let v_t be a time-varying collection of vector fields evaluated at time t:

$$\frac{\partial \psi_t(\boldsymbol{r})}{\partial t} = v_t(\psi_t(\boldsymbol{r})) \tag{1}$$

Potential energy. To drive registration, we use a potential term which is a three-dimensional equivalent of the energy formulation proposed for optical flow in [13]. Let U be the potential energy, Ω the image domain and w_{reg} the regularisation weight. We have:

$$U(\psi) = E_{\text{data}}(\psi) + w_{\text{reg}} E_{\text{reg}}(\psi) \tag{2}$$

$$= \frac{1}{2} \int_{\Omega} (\phi_{\text{source}}(\psi(\boldsymbol{r})) - \phi_{\text{target}}(\boldsymbol{r}))^2 \mathrm{d}\boldsymbol{r} + \frac{1}{2} w_{\text{reg}} \int_{\Omega} |\nabla \psi(\boldsymbol{r})|^2 \mathrm{d}\boldsymbol{r} \tag{3}$$

The potential consists of a data term E_{data}, which ensures similarity between the volumes based on image intensities, and a classical Tikhonov regularisation term E_{reg}, which imposes smooth motion.

Kinetic energy. In addition to the potential energy U discussed above, we define a kinetic energy T on the space of diffeomorphisms.

To define the kinetic energy we require mass. We represent it with a mass density $\rho : \mathbb{R}^n \to \mathbb{R}$, which corresponds to an infinite number of particles in $\mathbb{R}^n$, and which is evolved with the velocity field $\boldsymbol{v}$. Let $\rho_0 \in \mathbb{R}$. We have $\rho(\boldsymbol{r}) = \rho_0$. The mass density is evolved in time according to the continuity equation:

$$\frac{\partial \rho(\boldsymbol{r})}{\partial t} + \operatorname{div}(\rho(\boldsymbol{r})v(\boldsymbol{r})) = 0 \tag{4}$$

The continuity equation states that the rate at which mass enters a voxel is equal to the rate at which mass leaves the neighbouring voxels.

These assumptions allow us to define the kinetic energy of the system as follows:

$$T(v) = \int_{\phi(\mathbb{R}^n)} \frac{1}{2}\rho(\boldsymbol{r})|v(\boldsymbol{r})|^2 \mathrm{d}\boldsymbol{r} \tag{5}$$

It is the same as the definition of mass density which arises in fluid dynamics. It is worth noting that other designs of the kinetic energy may be used here, leading to an accelerated optimisation scheme with different dynamics, desirable e.g. in case of multi-channel images.

Action integral. The definitions of the potential U and the kinetic energy T let us define the Lagrangian of the system. To ensure convergence to a local minimum of the energy functional, we also need to consider energy dissipation. Let $a, b : [0, \infty] \to \mathbb{R}^+$. We define the action integral which describes the dynamics of the system as follows:

$$A = \int [a_t T(v_t) - b_t U(\phi_t)] dt \tag{6}$$

Velocity field. We set $a(t) = t^3/2$ and $b(t) = 2t$. This leads to the following evolution equation for the velocity field:

$$\frac{\partial \boldsymbol{v}}{\partial t} = -\frac{3}{t}\boldsymbol{v} - (D\boldsymbol{v})\boldsymbol{v} - \frac{1}{\rho}\nabla U(\psi) \tag{7}$$

where $D\boldsymbol{v}$ is the Jacobian of the velocity field and $\nabla U(\psi)$ is the variational gradient of the potential on the warped domain.

The term $-(3/t)\boldsymbol{v}$ functions as a frictional dissipative term, analogous to viscous resistance in fluids.

To further enhance the robustness of our method to shallow local minima of the energy functional, we use a simple heuristic and we add a diffusion term to the velocity update. Let τ be the diffusion coefficient:

$$\frac{\partial \boldsymbol{v}}{\partial t} = -\frac{3}{t}\boldsymbol{v} - (D\boldsymbol{v})\boldsymbol{v} + \tau\Delta\boldsymbol{v} - \frac{1}{\rho}\nabla U(\psi) \tag{8}$$

Large values of τ result in a preference for coarse-scale deformations in the early stages of optimisation, producing an effect similar to Sobolev gradients [30]. We

have observed that due to noise in the data velocity diffusion is essential from the perspective of optimisation to output an accurate deformation field but adds little computational cost.

With the added diffusion term, the equation becomes very similar to the incompressible Navier-Stokes equation in convective form. It only differs in the frictional term $-(3/t)\boldsymbol{v}$, which we use for energy dissipation.

Inverse deformation. The velocity field allows us to compute analytically not only the forward deformation ψ but also the inverse deformation ψ^{-1}. It is given by:

$$\frac{\partial \psi_t^{-1}}{\partial t} + [D\psi_t^{-1}(\boldsymbol{r})]\boldsymbol{v}_t(\boldsymbol{r}) = 0 \tag{9}$$

Energy gradient. Given the definition (2) of the potential $U(\psi)$, the gradient of the potential on the un-warped domain can be calculated as:

$$\nabla U(\psi) = [(\phi_{\text{source}} - \phi_{\text{target}} \circ \psi^{-1})\nabla\phi_{\text{source}} - w_{\text{reg}}(\Delta\psi) \circ \psi^{-1}]\text{det}\nabla\psi^{-1} \tag{10}$$

where $\nabla\phi_{\text{source}}$ is the spatial gradient of the image ϕ_{source} and $\Delta\psi$ is the Laplacian of ψ.

Implementation details. Eq. (4), (8), (1), and (9) completely describe our model and allow us to compute the required deformation by integrating them in time. Updates to the mass density ρ as well as the velocity $\boldsymbol{v}$ and the deformation fields ψ and ψ^{-1} are all local, so we can process all voxels independently and in parallel. This makes the accelerated optimisation scheme well-suited for a GPU implementation.

We use the default parameters $\rho_0 = 1$, $\Delta t = 0.004$, $\tau = 0.2$, and $w_{\text{reg}} = 0.2$. The value of ρ_0 is chosen heuristically to ensure sufficient regularity of the solution whilst giving the transformation model enough capacity to recover fine-scale details. We initialise $\psi(\boldsymbol{r}) = \psi^{-1}(\boldsymbol{r}) = \boldsymbol{r}$ and $\boldsymbol{v}(\boldsymbol{r}) = (0, 0, 0)$. The solver is run for a maximum number of 2048 iterations.

Due to lack of explicit spatial smoothing, correct setting of the regularisation weight w_{reg} is crucial to ensure accurate and meaningful registration. However, as w_{reg} and the diffusion coefficient τ are increased, the Courant-Friedrichs-Lewy (CFL) conditions due to the second-order terms in the form of the Laplacian of the deformation and velocity fields begin to dominate in the numerical implementation of the PDEs and necessitate smaller time steps.

5 Evaluation

In order to evaluate FastReg, we tested our system on two datasets of CT and MRI scans.

The first one is a publicly available dataset of abdominal CT scans[5]. In [39], the same dataset was used for the comparison of a number of non-rigid registration tools: FSL, ANTs-CC and ANTs-QUICK-MI, IRTK, Nifty-Reg, and

[5] https://www.synapse.org/#!Synapse:syn3193805/wiki/89480

DEEDS. It is worth noting that the evaluation in [39] was carried out with parameters optimised for the data by the authors of the software packages. The dataset consists of clinically acquired CT images with aligned segmentation masks. Thirteen abdominal organs were considered regions of interest (ROIs) for the segmentation, including spleen, right kidney, left kidney, gallbladder, esophagus, liver, stomach, aorta, inferior vena cava, portal and splenic vein, pancreas, left adrenal gland, and right adrenal gland. The ROIs were manually labelled by two undergraduate students, with the segmentations later verified by an experienced radiologist.

For each target image among the 21 scans, we performed cross-subject registration where the remaining 20 scans were used as source images to the target image in a pair-wise manner. As baseline affine registration have been shown to affect the efficacy of non-rigid registration methods [16,39], we performed rigid registration prior to non-rigid using the Nifty-Reg implementation of the block-matching algorithm, running only rigid registration, without the affine part. Rigid registration failed in approx. 25% of cases. For this reason, we include in our analysis only the 293 results where the rigid part of the pipeline succeeded out of 420 total registrations.

The second dataset consists of 15 clinically acquired brain MRI scans. Five tissues and structures were considered ROIs for the segmentation, including grey matter, white matter, cerebrospinal fluid, lateral ventricles, and brain stem. The ROIs were labelled by trained image analysis professionals. We registered each target image among the 15 scans, where the remaining 14 scans were used as source images to the target image in a pair-wise manner.

To test registration accuracy, we used the Dice coefficient, measuring the volumetric overlap between the estimated and the ground truth segmentations. On brain MRI we additionally measured the Hausdorff distance from the segmentation to the ground truth averaged for all ROIs.

Results. Figure 2 shows the Dice score values on 11 organs for the output of our method on the abdominal CT data. It can be compared to Figure 3 in [39]. Table 1 presents the overall performance of the method averaged across all organs, alongside results from [39].

On the brain MRI dataset, we asked the author of DEEDS for help registering the images using their software. Table 2 shows the average performance of FastReg and DEEDS on all the registrations and the five ROIs. Figure 3 shows an example registration.

6 Discussion

Runtime. To process the abdominal CT scans, we required approx. 14GB of GPU memory. For this reason, our code was run on a machine with an Nvidia Tesla P40 with 24GB of memory. Smaller image dimensions would allow to speed up registration, not only due to reduced dimensionality of the problem but also the fact that cheaper GPUs with less memory tend to offer higher clock rates.

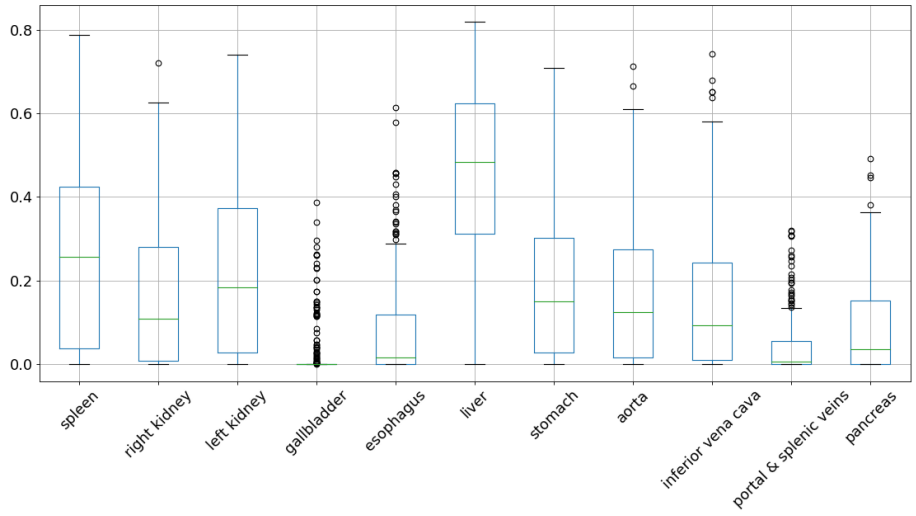

Fig. 2: Dice score values. Boxplot of DSC values on 11 organs for the output of our registration method.

At a resolution of $128 \times 128 \times 128$ voxels and using a machine with an Nvidia GeForce RTX 2080Ti, we are able to register up to seven image pairs per second.

Accuracy. In terms of accuracy, our method is on par with the state-of-the-art on the challenging task of registration of abdominal CT scans. Only DEEDS performs better than our scheme in terms of the Dice score. It was originally developed for registration of lung CT scans, which makes it well-suited also to cross-subject registration of abdominal CT data, with large deformations of small organs, sliding motion between organs, and changing image contrast. On brain MRI data, where such deformations are not prevalent, the gap between FastReg and DEEDS is much smaller. Moreover, our method is adaptable to any kind of medical and non-medical data, and more generally any non-convex optimisation problem.

The results here are based on a single similarity metric and we have not used other possible similarity metrics within the proposed scheme. It is possible to integrate cross-correlation, modality-independent neighbourhood descriptors (MIND) [10], or self-similarity context (SSC) [12] into the data term metric, which would likely change the measured accuracy of the framework.

Limitations. Similarly to previous algorithms, on abdominal CT, the proposed method registers large organs, such as liver and kidneys, with higher accuracy than smaller organs, e.g. gallbladder. Registration of smaller organs in the abdomen is an area with potential for further research.

Like all other non-rigid registration methods, FastReg struggles with very large deformations. This is due to the CFL conditions on the step size Δt, which needs to be made smaller with increasing maximum norm of the velocity field

Table 1: Metrics on 400 abdominal CT registrations as evaluated in [39]. We can see that FastReg compares favourably to other non-rigid registration methods. Note that the evaluation of all methods except FastReg was performed in [39] on a system with *twelve* 2.8GHz cores and 48 GB RAM, whereas we measured the runtime of FastReg on a system with *four* 3.6GHz cores, 32GB of RAM, and a Tesla P40 GPU.

Method	**DSC**	**Time (min)**
ANTs-CC [1]	0.18 ± 0.21	411.60 ± 74.20
ANTs-QUICK-MI [1]	0.27 ± 0.25	50.18 ± 21.93
DEEDS [12,9]	$\mathbf{0.49 \pm 0.26}$	3.73 ± 0.77
FastReg (our method)	0.36 ± 0.17	$\mathbf{1.78 \pm 0.01}$
FSL [38]	0.12 ± 0.19	951.73 ± 201.20
IRTK [27]	0.28 ± 0.26	220.27 ± 91.79
Nifty-Reg [22]	0.35 ± 0.29	116.91 ± 34.94

Table 2: Metrics on brain MRI registrations. In the absence of sliding motion between organs, the gap in registration accuracy between FastReg and DEEDS as measured with the Dice score is much smaller. Here the runtime comparison was performed on the same system with four 3.6GHz cores, 32GB of RAM, and a GeForce RTX 2080Ti GPU.

Method	**DSC**	**HD (mm)**	**Time (s)**
Before rigid registration	0.44 ± 0.07	21.36 ± 4.56	N/A
After rigid registration	0.60 ± 0.04	14.76 ± 4.56	N/A
DEEDS	$\mathbf{0.73 \pm 0.01}$	$\mathbf{13.72 \pm 2.27}$	50.52 ± 3.42
FastReg (our method)	0.67 ± 0.04	14.73 ± 2.67	$\mathbf{34.29 \pm 0.08}$

vector and of the components of the velocity field Jacobian. The update scheme underlying the method relies on forces based on image gradients, which are local in their scope. The typical response of a multilevel scheme, to capture larger deformations at a higher resolution, would not solve the local scope of the gradient-based update scheme.

The step size Δt can be dynamically adjusted based on its analytical upper bound. However, for large deformations this upper bound is likely to become infeasibly small, below machine precision. In theory, demons-based methods enable to capture more complex and larger deformations. We do not not compare our method to demons-based methods due to lack of a standard benchmark with parameters optimised to the data.

7 Conclusion

In this paper we have presented a new, elegant method for non-rigid diffeomorphic image registration which is based on accelerated optimisation on the

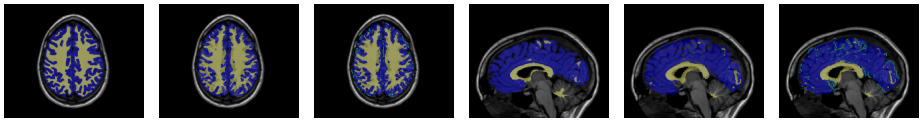

(a) **(b)** **(c)** **(d)** **(e)** **(f)**

Fig. 3: Example registration of a pair of brain MRI scans.. Blue—grey matter, yellow—white matter. (a) & (d): ϕ_{target} with the ground truth segmentation; (b) & (e): ϕ_{target} with the segmentation from the *rigid* registration of ϕ_{source}; (c) & (f): ϕ_{target} with the segmentation from the *non-rigid* registration of ϕ_{source} using FastReg. Difference between the non-rigid and rigid registrations highlighted in green.

manifold of diffeomorphisms. The proposed approach is problem-agnostic and leads to registrations of higher quality than related techniques, at faster speeds. It also shows promise for use in other image processing tasks. FastReg is a step forward towards faster and more general accurate medical image registration, leveraging recent advances in optimisation research.

In the future we will explore the choice of functions used for energy dissipation in order to achieve a better convergence rate for our problem. A data-driven analysis of the trade-off between the momentum and the gradient at each iteration of the solver is likely to improve robustness of the model to noise. We will also study the possibility of applying deep learning to refine the estimate of the flow. Deep learning models for computing optical flow could be used to provide an initial guess for the scheme and a better initialisation would likely allow to improve the final estimate of the variational scheme.

Acknowledgements. D. Grzech is funded by the EPSRC CDT in Medical Imaging EP/L015226/1. This research is supported by Intel, EPSRC EP/S013687/1 (MAVEHA), EPSRC EP/P023509/1, and Nvidia.

References

1. Avants, B.B., Tustison, N., Song, G.: Advanced normalization tools (ANTS). Insight j **2**, 1—-35 (2009)
2. Beg, M.F., Miller, M.I., Trouvé, A., Younes, L.: Computing large deformation metric mappings via geodesic flows of diffeomorphisms. Int. J. Comput. Vis. **61**(2), 139–157 (2005)
3. Charpiat, G., Maurel, P., Pons, J.P., Keriven, R., Faugeras, O.: Generalized gradients: Priors on minimization flows. Int. J. Comput. Vis. **73**(3), 325–344 (2007)
4. Crum, W.R., Hartkens, T., Hill, D.L.G.: Non-rigid image registration: theory and practice. Br. J. Radiol. **77**, S140–S153 (2004)
5. Dosovitskiy, A., Fischery, P., Ilg, E., Hausser, P., Hazirbas, C., Golkov, V., Smagt, P.V.D., Cremers, D., Brox, T.: FlowNet: Learning optical flow with convolutional networks. Proc. IEEE Int. Conf. Comput. Vis. **2015 Inter**, 2758–2766 (2015)
6. Duchi, J., Hazan, E., Singer, Y.: Adaptive Subgradient Methods for Online Learning and Stochastic Optimization. J. Mach. Learn. Res. **12**, 2121–2159 (2011)

7. Ebin, D.G., Marsden, J.: Groups of Diffeomorphisms and the Motion of an Incompressible Fluid. Ann. Math. **92**(1), 102 (1970)
8. Glocker, B., Komodakis, N., Tziritas, G., Navab, N., Paragios, N.: Dense image registration through MRFs and efficient linear programming. Med. Image Anal. **12**(6), 731–741 (2008)
9. Heinrich, H.P., Jenkinson, M., Brady, M., Schnabel, J.A.: MRF-Based Deformable Registration and Ventilation Estimation of Lung CT. IEEE Trans. Med. Imaging **32**(7), 1239–1248 (jul 2013)
10. Heinrich, M.P., Jenkinson, M., Bhushan, M., Matin, T., Gleeson, F.V., Brady, S.M., Schnabel, J.A.: MIND: Modality independent neighbourhood descriptor for multi-modal deformable registration. Med. Image Anal. **16**(7), 1423–1435 (2012)
11. Heinrich, M.P., Simpson, I., Papiez, B.W., Brady, M.J., Schnabel, J.A.: Deformable image registration by combining uncertainty estimates from supervoxel belief propagation. Med. Image Anal. **27**, 57–71 (2015)
12. Heinrich, M.P., Jenkinson, M., Papież, B.W., Brady, S.M., Schnabel, J.A.: Towards Realtime Multimodal Fusion for Image-Guided Interventions Using Self-similarities. In: Mori, K., Sakuma, I., Sato, Y., Barillot, C., Navab, N. (eds.) Med. Image Comput. Comput. Interv. 2013. pp. 187–194. Springer Berlin Heidelberg, Berlin, Heidelberg (2013)
13. Horn, B.K., Schunck, B.G.: Determining Optical Flow. Artif. Intell. **17** (1980)
14. Ilg, E., Mayer, N., Saikia, T., Keuper, M., Dosovitskiy, A., Brox, T.: FlowNet 2.0: Evolution of Optical Flow Estimation with Deep Networks (2016)
15. Kazemi, P., Danaila, I.: Sobolev Gradients and Image Interpolation. SIAM J. Imaging Sci. **5**(2), 601–624 (2012)
16. Lee, C.P., Xu, Z., Burke, R.P., Baucom, R.B., Poulose, B.K., Abramson, R.G., Landman, B.A.: Evaluation of Five Image Registration Tools for Abdominal CT: Pitfalls and Opportunities with Soft Anatomy HHS Public Access. Proc SPIE Int Soc Opt Eng **9413** (2015)
17. Lorenzi, M., Ayache, N., Frisoni, G., Pennec, X.: LCC-Demons: A robust and accurate symmetric diffeomorphic registration algorithm. Neuroimage **81**, 470–483 (2013)
18. Lorenzi, M., Pennec, X., Frisoni, G.B., Ayache, N.: Disentangling normal aging from Alzheimer's disease in structural magnetic resonance images. Neurobiol. Aging **36**, S42–S52 (jan 2015)
19. Lötjönen, J.M., Wolz, R., Koikkalainen, J.R., Thurfjell, L., Waldemar, G., Soininen, H., Rueckert, D.: Fast and robust multi-atlas segmentation of brain magnetic resonance images. Neuroimage **49**(3), 2352–2365 (2010)
20. Maddison, C.J., Paulin, D., Teh, Y.W., Doucet, A.: Hamiltonian Descent Methods (2018)
21. Makropoulos, A., Robinson, E.C., Schuh, A., Wright, R., Fitzgibbon, S., Bozek, J., Counsell, S.J., Steinweg, J., Vecchiato, K., Passerat-Palmbach, J., Lenz, G., Mortari, F., Tenev, T., Duff, E.P., Bastiani, M., Cordero-Grande, L., Hughes, E., Tusor, N., Tournier, J.D., Hutter, J., Price, A.N., Teixeira, R.P.A., Murgasova, M., Victor, S., Kelly, C., Rutherford, M.A., Smith, S.M., Edwards, A.D., Hajnal, J.V., Jenkinson, M., Rueckert, D.: The developing human connectome project: A minimal processing pipeline for neonatal cortical surface reconstruction. Neuroimage **173**, 88–112 (jun 2018)
22. Modat, M., Ridgway, G.R., Taylor, Z.A., Lehmann, M., Barnes, J., Hawkes, D.J., Fox, N.C., Ourselin, S.: Fast free-form deformation using graphics processing units. Comput. Methods Programs Biomed. **98**(3), 278–284 (2010)

23. Nesterov, Y.: Smooth minimization of non-smooth functions. Math. Program. **103**(1), 127–152 (2005)
24. Ou, Y., Ye, D.H., Pohl, K.M., Davatzikos, C.: Validation of DRAMMS among 12 Popular Methods in Cross-Subject Cardiac MRI Registration. Biomed Image Regist Proc. **7359**, 209–219 (jul 2012)
25. Rueckert, D., Sonoda, L.I., Hayes, C., Hill, D.L.G., Leach, M.O., Hawkes, D.J.: Nonrigid Registration Using Free-Form Deformations: Application to Breast MR Images. IEEE Trans. Med. Imaging **18**(8), 712–721 (1999)
26. Schnabel, J.A., Heinrich, M.P., Papiez, B.W., Brady, J.M.: Advances and challenges in deformable image registration: From image fusion to complex motion modelling. Med. Image Anal. **33**, 145–148 (2016)
27. Schnabel, J.A., Rueckert, D., Quist, M., Blackall, J.M., Castellano-Smith, A.D., Hartkens, T., Penney, G.P., Hall, W.A., Liu, H., Truwit, C.L., Gerritsen, F.A., Hill, D.L.G., Hawkes, D.J.: A Generic Framework for Non-rigid Registration Based on Non-uniform Multi-level Free-Form Deformations. In: Niessen, W.J., Viergever, M.A. (eds.) Med. Image Comput. Comput. Interv. 2001. pp. 573–581. Springer Berlin Heidelberg, Berlin, Heidelberg (2001)
28. Slavcheva, M., Baust, M., Cremers, D., Ilic, S.: KillingFusion: Non-rigid 3D Reconstruction without Correspondences. 2017 IEEE Conf. Comput. Vis. Pattern Recognit. pp. 5474–5483 (2017)
29. Slavcheva, M., Baust, M., Cremers, D., Ilic, S.: KillingFusion: Non-rigid 3D Reconstruction without Correspondences: Supplementary material. 2017 IEEE Conf. Comput. Vis. Pattern Recognit. pp. 5474–5483 (2017)
30. Sundaramoorthi, G., Yezzi, A.: Accelerated Optimization in the PDE Framework: Formulations for the Manifold of Diffeomorphisms (2018)
31. Sundaramoorthi, G., Yezzi, A., Mennucci, A.: Sobolev Active Contours. In: Paragios, N., Faugeras, O., Chan, T., Schnörr, C. (eds.) Var. Geom. Lev. Set Methods Comput. Vis. pp. 109–120. Springer Berlin Heidelberg, Berlin, Heidelberg (2005)
32. Sundaramoorthi, G., Yezzi, A., Mennucci, A.C.: Sobolev active contours. Int. J. Comput. Vis. **73**(3), 345–366 (2007)
33. Thirion, J.P.: Image matching as a diffusion process: An analogy with Maxwell's demons. Med. Image Anal. **2**(3), 243–260 (1998)
34. Urschler, M., Werlberger, M., Scheurer, E., Bischof, H.: Robust Optical Flow Based Deformable Registration of Thoracic CT Images (2010)
35. Vercauteren, T., Pennec, X., Malis, E., Perchant, A., Ayache, N.: Insight into Efficient Image Registration Techniques and the Demons Algorithm. In: Inf. Process. Med. Imaging. vol. 20, pp. 495–506. Springer (2007)
36. Vercauteren, T., Pennec, X., Perchant, A., Ayache, N.: Diffeomorphic demons: efficient non-parametric image registration. Neuroimage **45**(1 Suppl), S61—-S72 (2009)
37. Wibisono, A., Wilson, A.C., Jordan, M.I.: A Variational Perspective on Accelerated Methods in Optimization. Proc. Natl. Acad. Sci. **113**(47), 1–38 (nov 2016)
38. Woolrich, M.W., Jbabdi, S., Patenaude, B., Chappell, M., Makni, S., Behrens, T., Beckmann, C., Jenkinson, M., Smith, S.M.: Bayesian analysis of neuroimaging data in FSL . Neuroimage **45**, S173–S186 (2008)
39. Xu, Z., Lee, C.P., Heinrich, M.P., Modat, M., Rueckert, D., Ourselin, S., Abramson, R.G., Landman, B.A.: Evaluation of Six Registration Methods for the Human Abdomen on Clinically Acquired CT. IEEE Trans Biomed Eng **63**(8), 1563–1572 (2016)
40. Zeiler, M.D.: ADADELTA: An Adaptive Learning Rate Method (2012)